Progress In Electromagnetics Research, Vol. 128, 347–363, 2012

PATH-LOSS PREDICTION OF RADIO WAVE PROPAGATION IN AN ORCHARD BY USING MODIFIED UTD METHOD

K. Phaebua[1], C. Phongcharoenpanich[1, *], M. Krairiksh[1], and T. Lertwiriyaprapa[2]

[1]Faculty of Engineering, King Mongkut's Institute of Technology Ladkrabang, 1 Chalongkrung Road, Ladkrabang, Bangkok 10520, Thailand

[2]Department of Teacher Training in Electrical Engineering, Faculty of Technical Education, King Mongkut's University of Technology North Bangkok, 1518 Piboonsongkarm Road, Bangsue, Bangkok 10800, Thailand

Abstract—In this paper, the proposed theoretical path-loss prediction procedure and measured results of radio wave propagation in an orchard environment are presented. The path-loss prediction of wireless sensor network (WSN) in a durian (*Durio zibethinus Murray*) orchard is chosen to be an example of this study. The three-dimensional (3-D) modified uniform geometrical theory of diffraction (UTD) for curved impedance surface and the complex source point (CSP) technique for source modeling are employed for theoretical path-loss prediction in this paper. The orchard scenario is modeled using canonical geometries of UTD, such as a dielectric flat surface and cylindrical structures with an impedance surface to respectively represent ground and trees. Moreover, since the wireless sensor node is attached to the outside peel of a hanging durian fruit, the fruit partially acts as a wireless sensor node. Therefore, to obtain greater accuracy in the source radiation pattern, the Gaussian beam (GB) expansion via the CSP technique is used for source modeling. The path loss prediction from the proposed numerical procedure and the measured results are in good agreement. The proposed numerical procedure to calculate the path loss from actual scenario of the orchard is useful for network planning such as the pre-harvesting WSN system and other orchard scenarios.

Received 1 April 2012, Accepted 21 May 2012, Scheduled 2 June 2012

* Corresponding author: Chuwong Phongcharoenpanich (pchuwong@gmail.com).

1. INTRODUCTION

The demand for wireless communication systems, such as the mobile phone systems and Wireless Sensor Network (WSN), has been continuously on the increase due to their wireless connection advantages. Every WSN application requires its specific radio wave propagation channel in each scenario for the network planning. Of the mobile phone application in the large communication area with very high transmitting antennas and tall obstacles in the line-of-sight path, the empirical models of radio wave propagation are efficiently employed [1]. However, most of the empirical models in [2–4] are dependent upon scenarios. For instance, the two-ray model is valid for use in the case of strong reflection from the ground, and the Weissberger model can be used in the forest setting to predict the path loss of wave propagation. Besides, Chen and Kua proposed a model using vertical/horizontal polarizations for a forest. In such WSN applications, the transmitted power of WSN systems is very low, thus the coverage area being relatively small. The transmitting antennas are located a few meters above the ground and the geometries of the environment such as buildings and ground have strong effects on the receiving power at the receiving points. As such, the wave propagation prediction requires a more accurate method to predict the signal strength in its respective scenario. An efficient method for the wave propagation prediction is the uniform geometrical theory of diffraction (UTD) [5–10] (i.e., analytical solution) while numerical methods are less efficient or unsuited to the propagation problems because the computation domain of the latter is very large in comparison with the electrical wavelength. The analytical solution based on the Sommerfeld integrals method was presented in [11], but the UTD method was instead used in this study since it is less complicated than the Sommerfeld integrals method. In addition, the UTD method provides the physical insight that allows one to quantitatively, separately study the effects of field types at the observation point, while numerical methods require more efforts to extract the propagation mechanisms such as that presented in [12]. Unlike the empirical model, the analytical solution does not require any measurement for path-loss data to construct the path-loss model of each scenario. Only the actual geometry of the orchard such as positions, diameters of the trees, and properties of the ground are required in the analytical procedure. The UTD solution has been widely used in the propagation predictions [1, 5, 9, 10] and [13–15] under an assumption that the surface is perfectly electric conductor (PEC). However, the PEC surface model is efficient when used in the case of strong reflection and diffraction from the obstacle. The UTD

solutions for planar impedance surface configurations were studied in [16] and [17]. The 2-D UTD solutions for the curved impedance surface were presented in [18] and [19]. However, the 2-D UTD solutions for the curved impedance surface do not support 3-D scenario.

This paper presents an application of the modified 3-D UTD for the curved impedance surface in [20] for the path loss prediction of the WSN system in an orchard. In this research, a durian orchard is chosen to be a pioneering example of the WSN for fruit maturity monitoring system. The proposed numerical procedure obtained from this work is applicable to other types of orchards, such as rubber tree orchard, palm orchard, coconut orchard and other plantations for logging, with nevertheless slight changes in such physical properties of the orchard as tree size, locations of the trees, tree barks, ground types, and wave source. Besides monitoring ripening of the fruits, WSN can be used in fire monitoring system, water monitoring [21] and control system. However, it is difficult to create a model that represents every influencing factor detected in the orchard, such as the reflection and diffraction from leaves and tree branches. Because of the short communication distance in the orchard and the proximity of the transmitting and receiving antennas to the ground, merely the rays from tree trunks and the ground are studied. The durian trees in the orchard are modeled using impedance cylindrical surface structures. The orchard ground is modeled using the dielectric ground containing the relative permittivity ε_r, the relative permeability μ_r and the conductivity σ. The modified 3-D UTD scattering solution for impedance cylinder presented in [20] is obtained by heuristically modifying the classical 3-D UTD solution for a PEC curved surface [7] with impedance Pekeris' caret function [18] and [22]. Moreover, the Guassian beam (GB) expansion method based on the Complex source point (CSP) technique to synthesize the radiation pattern of source is employed. The expansion of the GBs is effectively used to generate the radiation pattern. It should be noted that in this work all fields are assumed with $e^{j\omega t}$ time dependence and suppressed throughout.

2. ORCHARD AND SOURCE MODELING

Photographs of the orchard (Horticultural Research Center (HRC), Thailand) and a durian fruit are illustrated in Figs. 1 and 2, respectively. Typically, the height and diameter of durian trees, depending upon their species, are more than 10 meters (32.8 feet) and approximately 0.3 meter (12 inches), respectively. The proposed model is created under the assumption of no branches and leaves because as shown in Fig. 1(a) durian trees in the plantation have a small number of

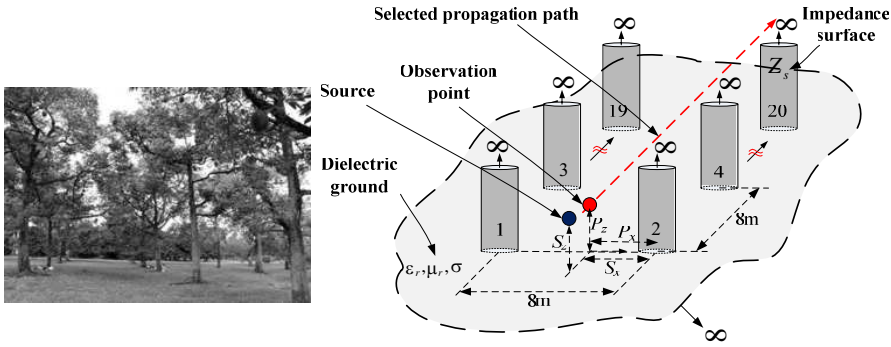

Figure 1. Orchard modeling: (a) Durian orchard, (b) model of the orchard using the canonical structure.

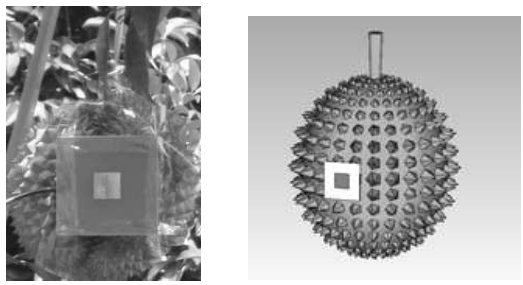

Figure 2. (a) Vertical polarized patch antenna on a durian fruit. (b) Drawing of patch antenna on a durian fruit.

branches and leaves near the ground. In this study, the geometry of the durian trees is replaced with canonical shapes such as a simple cylinder with an impedance surface, and the actual ground with the dielectric planar surface [23]. The proposed model of the durian orchard is shown in Fig. 1(b). Z_s denotes an impedance surface parameter of the cylinder, S_x the distance of source from cylinder No. 2, S_z the height of source above the ground, and a the durian tree radius.

It was found in [15] that the path-loss is strongly affected by the source pattern of the transmitting antenna. In the WSN system under the study, a sensor device (patch antenna) is first attached onto the exterior of a durian fruit as shown in Fig. 2 and the communication nodes of the WSN are then installed near the ground of the durian orchard. The chosen patch antenna provides a vertical polarization (V-polarized), unidirectional pattern and operating frequency at 2.45 GHz.

The radiation pattern from the patch antenna attached on the durian fruit is altered due to the shape of the durian fruit. Therefore, it is necessary to carefully model the actual source in the orchard modeling. The GB expansion via CSP technique can be efficiently applied to the UTD solution [24]. The GB expansion is employed to interpolate the radiation pattern from actual source as shown in Fig. 2.

3. THEORY

3.1. UTD Incident Field Via the GB Representation

The arbitrary GB directions in 3-D case can be generated using the CSP [25] and [26] as shown in Fig. 3(a). The amplitude of GB rapidly decays in the same fashion as the Gaussian function when the observation point moves away from the axis of the GB. It is found that the CSP beam expansion can efficiently represent electromagnetic radiation and scattering problems because the number of GB terms can be truncated by employing the rapid decaying property of the GB to reduce the computational time [27]. This is the main advantage of using the GB expansion rather than other expansions such as the spherical wave or plane wave expansions. The complex source location is obtained by substituting the real source location with complex source location, where the $\tilde{\bar{r}}'$, $\tilde{\phi}'$ and $\tilde{\bar{R}}$ are complex parameters. The beam waist of GB at origin of the CSP is defined as w_0, where θ_b and ϕ_b denote the GB direction angles. The $r = \sqrt{x^2 + y^2 + z^2}$ denotes the real distance of the observation points when $x = r\sin\theta\cos\phi$, $y = r\sin\theta\sin\phi$ and $z = r\cos\theta$. The real source location is defined as $x' = r'\sin\theta'\cos\phi'$, $y' = r'\sin\theta'\sin\phi'$ and $z' = r'\cos\theta'$. The complex source location can then be expressed as $\tilde{x'} = x' - jb\sin\theta_b\cos\phi_b$, $\tilde{y}' = y' - jb\sin\theta_b\sin\phi_b$ and $\tilde{z'} = z' - jb\cos\theta_b$, where $\tilde{r}' = \sqrt{\tilde{x}'^2 + \tilde{y}'^2 + \tilde{z}'^2}$. Thus, the distance between the source point and the observation point can be written as $\tilde{R} = r - \tilde{r'}$. To construct radiation pattern of source, the expansion of Gaussian beams can be expressed with

$$E\left(\tilde{R}\right) = \sum_{n=1}^{N} a_n \frac{e^{-jk\tilde{R}}}{\tilde{R}}. \tag{1}$$

The $E(\tilde{R})$ denotes the radiation pattern function at any observation point. The unknown sampling field coefficients of the total number of the GBs (N) are defined by a_n, which can be determined using point matching together with the actual source radiation pattern from measurement. Fig. 3(b) shows the equivalent sphere with radius $a_{eqv.} = 1$. The $\Delta\phi_b = \Delta\theta_b$ denotes the delta sampling angles of GB as

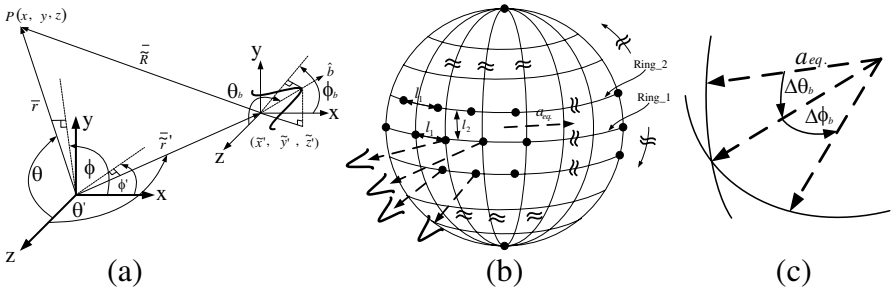

Figure 3. Antenna pattern representation: (a) CSP for constructing the GB, (b) the summation of arbitrary directions of GBs, (c) the spacing angles between GBs.

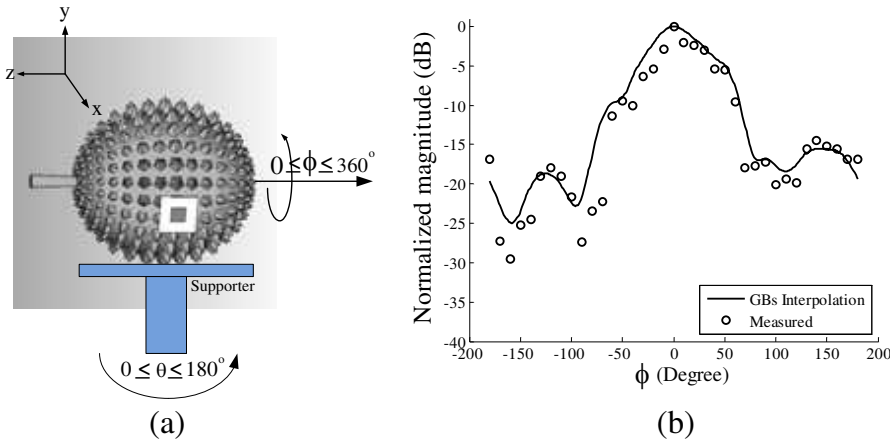

Figure 4. (a) The diagram of the radiation pattern measurement of the patch antenna on durian fruit. (b) 2-D source radiation pattern.

shown in Fig. 3(c). Thus, the number of GBs on the equivalent ring on the equivalent sphere varies depending upon the location of equivalent ring on the equivalent sphere. The GBs with different coefficients a_n are located at the origin of equivalent sphere.

As previously mentioned, the unknown coefficients a_n can be determined with point matching of the actual sampling field radiation pattern obtained from measurement. The patch antenna attached on the durian fruit is supported by the planar supporter made of polyurethane foam and wood as shown in Fig. 4(a). The sampling field was measured by varying in 10-degree incremental steps the θ and ϕ angles. Finally, the field strength (linear scale) is normalized to the maximum value to determine the GB coefficients a_n. Fig. 4(b)

shows the experiment and the synthesis of the normalized field pattern. The comparison indicates good agreement. In this work, to reduce the computational time, 10 degrees of the sampling angles and the beam waist of GB with 1λ are selected.

3.2. UTD Canonical Problem and Equations

Figure 5 shows all possible ray paths in the orchard model. Fig. 5(a) shows the cylindrical structure with 3-D diffracted ray paths, Fig. 5(b) illustrates all ray paths of a single cylinder at different regions, i.e., front and rear of the shadow boundary (SB), and Fig. 5(c) is the dielectric ground model and its reflected ray path. The actual ground is modeled using the dielectric ground model [23]. The total field, i.e., vertical polarization source, at the observation point of the proposed procedure consists of the incident field $u_i(P)$, the reflected field $u_r(P)$ from all of the impedance cylinders, the diffracted fields $u_d(P)$ from two sides of all impedance cylinders in the orchard model, and the reflected field from dielectric ground u_r^{ground}.

The total field u_t of the proposed procedure can be written as

$$u_t = u_t^{\text{lit}}(P) + u_d(P). \tag{2}$$

The u_t^{lit} is the field at the observation point P in the lit region which can be written as

$$u_t^{\text{lit}}(P) = u_i(P) + \underbrace{\sum_{m=1}^{M} u_i^m(Q_R^m) R_{s,h}^m A_{\text{lit}}^m e^{-jks_r^m}}_{\text{All reflected field from impedance cylinders}} + u_r^{\text{ground}} \tag{3}$$

where M denotes total number of impedance cylinders in the orchard model. It is noted that the results of actual radiation pattern obtained from the previous section using GB expansion technique are used as the incident field in this work. $R_{s,h}$ denotes the reflection coefficients of the curved surface, which consist of the Fresnel's function and the Pekeris' caret function. The subscripts s and h refer to soft (i.e., electric field incident parallel to the axis of cylinder) and hard polarizations (i.e., magnetic field incident parallel to the axis of cylinder) of the incident wave. A_{lit} represents the 3-D spreading factor in the lit zone conditional upon incident wave types and surface geometry. S_r denotes reflected path length of each impedance cylinder. The diffracted fields $u_d(P)$ from the surface Q_2 of all cylinders to the observation point P are shown in Figs. 5(a) and (b). The $u_d(P)$ of M cylinders can be written as

$$u_d(P) = \sum_{m=1}^{M} u_i^m(Q_1^m) T_{s,h}^m A_{\text{shadow}}^m e^{-jks_d^m}. \tag{4}$$

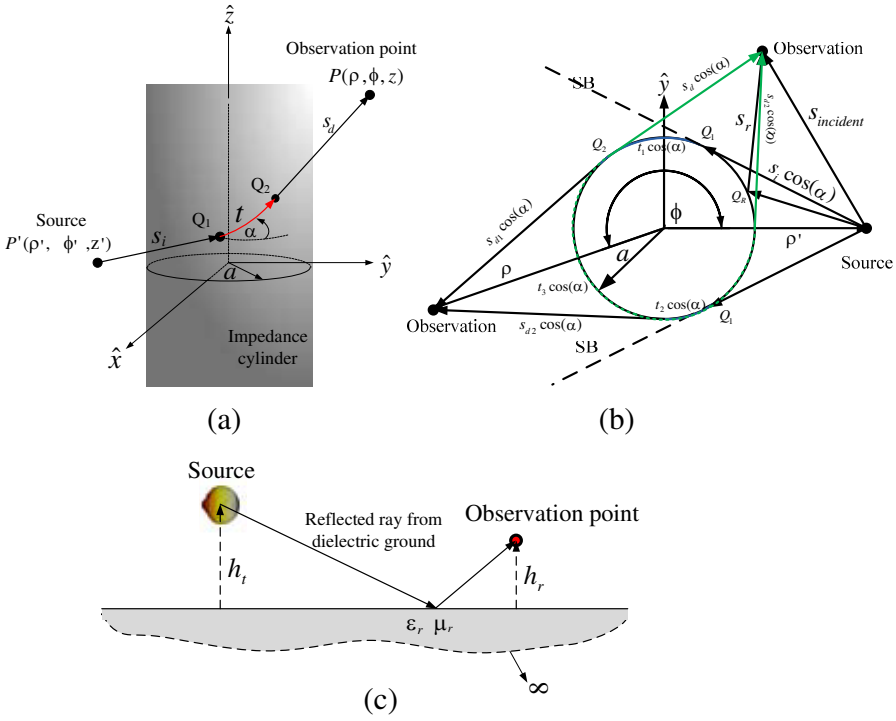

Figure 5. Geometrical modeling of a tree: (a) Tree model using impedance cylinder and diffracted ray paths, (b) ray mechanisms of a cylinder, (c) dielectric ground model and reflected ray path.

The $u_i\,(Q_1)$ denotes the incident field at the incident diffraction point Q_1 of each cylinder, and S_d denotes the diffracted path length. The transmission coefficients $T_{s,h}$ consisting of the Fresnel's function and the Pekeris' caret function can be numerically computed. A_{shadow} denotes the 3-D spreading factor in the shadow zone depending on the surface geometry. The parameters in Equations (3) and (4) can be found in [7], and the details of the modified 3-D UTD solution for an impedance cylinder surface are presented in [20].

Generally, the numerical scheme to calculate PEC Pekeris' caret integral function $P_{s,h}(\xi^L)$ is unavailable for a curved impedance surface. In this paper, the numerical integration based on the recursive adaptive Simpson Quadrature is applied. To verify the accuracy of the proposed idea using the numerical integration, the comparison between the proposed solution and the simulation results from the CST Microwave Studio program of single impedance cylinder is shown

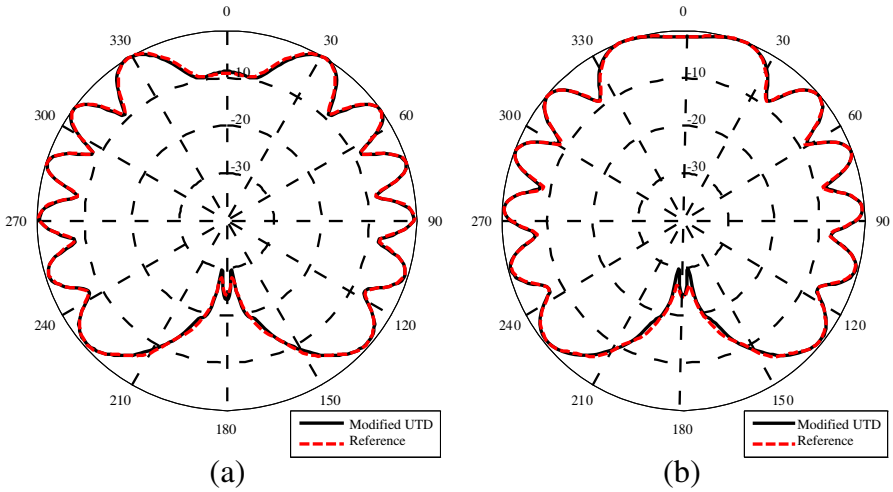

Figure 6. Comparison of the total field (vertical dipole source) between the modified UTD and CST Microwave Studio program (reference) versus ϕ angle: $a = 2\lambda$, $\rho' = 5\lambda$, $t = 0.06\lambda$, $\varepsilon_r = 4$, $\mu_r = 1$ and $\rho = 100\lambda$. (a) $\theta = 90°$ (2-D case). (b) $\theta = 70°$ (3-D case).

in Fig. 6. The value of surface impedance Z_S of the thinly coated cylinder derived from the approximation of the problems was presented in [28]. The axis of cylinder is located along z-axis. The θ angle is measured from z-axis to the observation point. It is noted that the proposed UTD solution can automatically recover the 2-D case when the incident angle becomes perpendicular to the cylinder axis. As shown in Fig. 6, the numerical results obtained from the proposed UTD solution were in line with the results from CST program for both normal (2-D case) and oblique (3-D case) incidents.

4. MEASUREMENT SETUP

The path-loss measurement was performed in a durian orchard of the Horticultural Research Center (HRC), Khlung, Chanthaburi, Thailand. The spacings between any two durian trees are horizontally and vertically 8 meters. The photographs of the measurement setup and the locations of transmitter and receiver are shown in Fig. 7. The average diameter of durian trees is 0.3 meter ($a = 0.15$ meter). The vertical polarized antennas for source and observation point are employed. The source antenna is attached on a durian fruit with $S_z = 2.2$ meters and $S_x = 1.5$ meters as shown in Fig. 7(b). The

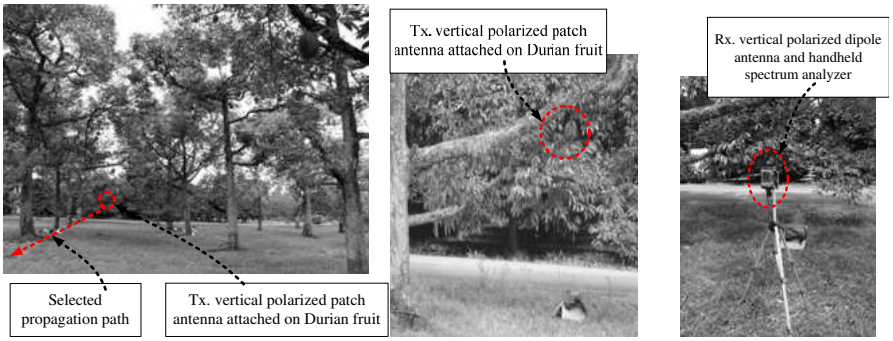

Figure 7. Measurement setup: (a) The propagation path view, (b) patch antenna on durian fruit and its location, (c) 2.45 GHz handheld spectrum analyzer.

handheld spectrum analyzer as shown in Fig. 7(c) is used to receive the field strength at the observation points along the measurement path. The receiving antenna is located at $P_z = 1.5$ meters and $P_x = 1.5$ meters as shown in Fig. 7(c). The overall distance of propagation measurement is 80 meters. The sampling distance for measurement of 4 meters was chosen along the propagation path.

5. NUMERICAL AND MEASURED RESULTS

Many research works have studied on the relative permittivity of the various species of wood [29] and [30]. In the measurement results presented in [29] and [30], at the percentage of moisture contents below 50%, the relative permittivity of wood of approximately $\varepsilon_r = (2 \text{ to } 6) - j(0.1 \text{ to } 2.828)$ depends on the percentage of moisture contents and structural direction of wood. Due to relative permittivity of the durian wood is unavailable, the value of the relative permittivity of the cylindrical surface of $\varepsilon_r = 4.77 - j2.828$ is used in this work, which comes from the measurement result of dielectric properties of the oriental beech species with moisture content 28% at microwave frequencies (2.45 GHz) in [29].

The dielectric constants of the various kinds of the actual ground have been reported in [23, 31, 32]. The average ground with $\sigma = 5 \times 10^{-3}$ S/m and $\varepsilon_r = 15$ represents the actual ground in this work. The distances between any two durian trees are horizontally and vertically 8 meters. The average radius of durian trees is 0.15 meter ($a = 0.15$ meter). $S_z = 2.2$ meters, $S_x = 1.5$ meters, $P_z = 1.5$ meters and

$P_x = 1.5$ meters. The overall distance for propagation measurement is 80 meters. The field distributions in the communication area (i.e., the rectangular area as shown in Fig. 8) normalized to the maximum value of all plots are shown in Fig. 9. Fig. 9(a) shows the total field distribution which consists of the incident ray and scattered rays from cylinders without reflected ray from ground. Fig. 9(b) shows the total field plot without scattered rays from impedance cylinders. Fig. 9(c) shows the total field distribution which consists of the incident ray, reflected ray from ground and scattered rays from cylinders (i.e., all possible ray paths of the proposed model). In Fig. 9(a), the scattered rays from cylinders significantly contribute to the total field in the far

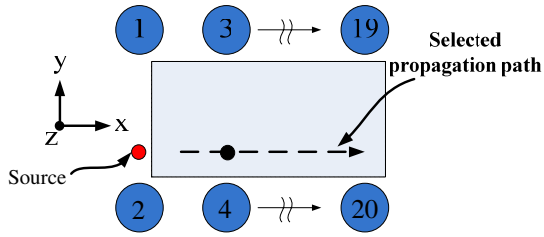

Figure 8. Selected area in the orchard modeling.

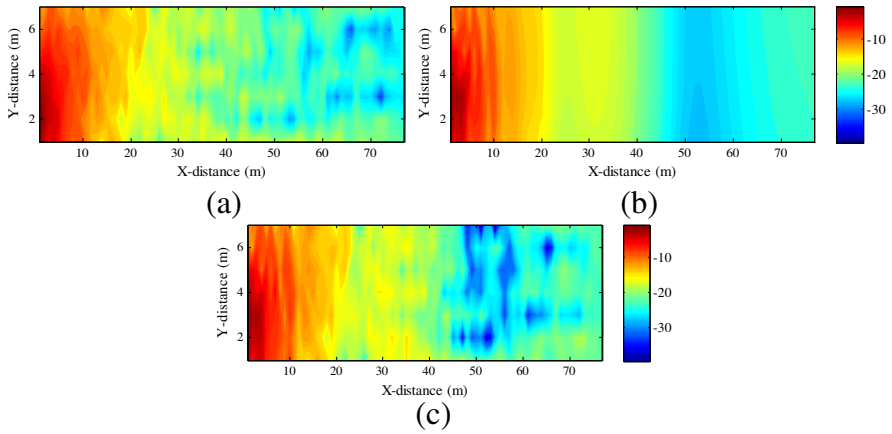

Figure 9. Normalized total field in the considered area: (a) Without reflected ray from ground (i.e., only incident ray and scattered rays from cylinders), (b) without scattered ray from cylinders (i.e., only incident ray and reflected ray from ground), and (c) normalized total field (i.e., incident ray, reflected ray from ground and scattered rays from cylinders).

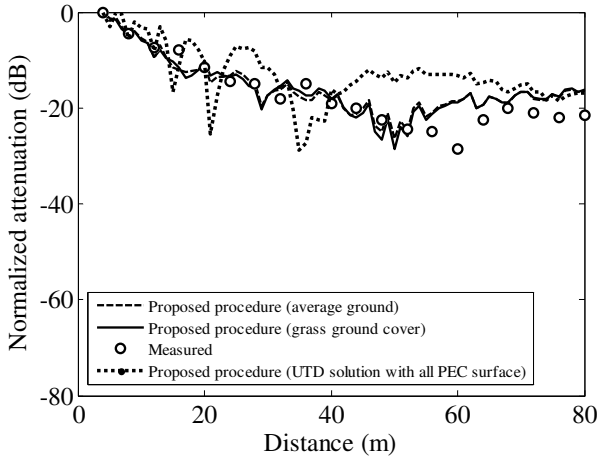

Figure 10. Comparison between path loss of the numerical and measured results at 2.45 GHz: Average ground ($\sigma = 5 \times 10^{-3}$ S/m and $\varepsilon_r = 15$) and grass-covered ground ($\sigma = 0.163$ S/m and $\varepsilon_r = 8$), both with impedance cylindrical surface ($\varepsilon_r = 4.7 - j2.828$ and $t = 0.06\lambda$) and with PEC surface.

region of the communication area. The total field strength in Fig. 9(a) is slightly changed when compared to that in Fig. 9(c) except in the 45–60 meters region. Fig. 9(b) shows the total field without scattered field from impedance cylinders. The reflected ray from ground is strong near the source and also show null of the total field in the region of 45–60 meters. The total field strength increases again in the region from 60 meters to 80 meters. Importantly, if the position of trees is not uniform in the orchard or the density of trees is changed, the field distribution plot of the total field strength in the communication area can be readily calculated using the proposed numerical procedure. However, under the same conditions, the total field strength cannot be computed with the empirical models [2–4]. This field distribution plot provides useful information as to the location to install the communication node around the sensor node (source) in the orchard. The plots in Fig. 9 show that the UTD solution provides physical insight of the problem since each field contribution can be quantitatively extracted.

Figure 10 shows the comparison between path loss of the numerical and measured results. The numerical results are calculated with two ground surface types and all PEC surfaces (i.e., ground and cylinders). The two ground surface types are average ground and grass-covered ground. In this paper, the impedance cylindrical surface of the oriental beech wood species [29] with $\varepsilon_r = 4.7 - j2.828$ is used in

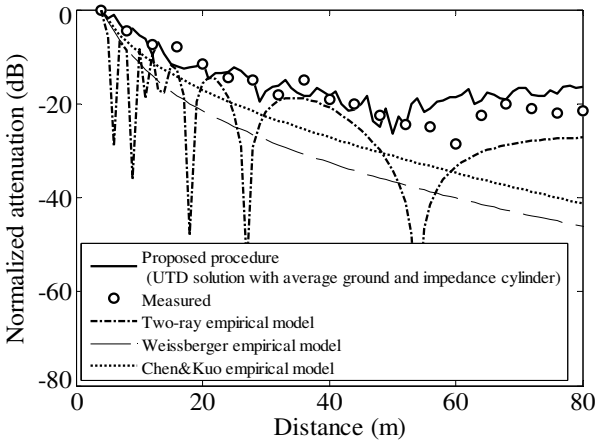

Figure 11. Comparisons of empirical models and path losses of the numerical and measured results at 2.45 GHz.

the proposed model. This value varies according to different wood surfaces. The dielectric coated thickness in the UTD model of 0.06λ is chosen. Nevertheless, the dielectric coated thickness, the radius a and position of the trees can be altered to suit different scenarios. The circle line is the measurement results along the propagation path of 80 meters sampling every 4 meters. In Fig. 10, the numerical results from the proposed UTD solution for the average ground, the grass-covered ground and all PEC surfaces are shown with the dashed line, the solid line and dotted line, respectively. The difference in numerical path loss predictions of two ground types is insignificant. Within the range of 4–50 meters, the numerical results show good agreement with the measured result. The prediction shows discrepancies in the range of 50–80 meters due to the incident field and reflected field dramatically decreasing in the far region. In fact, the multipath fading caused by multiple reflections from a group of leaves, surface wave of ground and multiple diffractions from trees is stronger than incident field from source and reflected field from ground at the far region. However, due to low transmitting power of both the sensor and communication nodes of the WSN, the communication range is usually limited to 40 meters or less. Therefore, the proposed method will be adequate for the proposed scenario. To improve the accuracy of path loss prediction at the far region in the future research, the proposed numerical procedure requires more field components such as the surface wave of dielectric ground and multiple reflections/diffractions from a group of leaves. Moreover, it is found that the field strength of all PEC surfaces (i.e.,

dotted line in Fig. 10) fluctuated along the propagation path due to strong constructive and destructive effects among incident field, reflected field from ground, and scattered fields from cylinders. This causes the reflection from ground and scattered field from cylinders in the PEC case to be stronger than in the case of impedance surface cylinders with dielectric ground. Therefore, the PEC surface model cannot be used to accurately predict the path loss in this scenario.

The comparison results in Fig. 11 are from the proposed solution and the empirical models for the forest. The two-ray model, Weissberger model and Chen & Kua model are presented in the empirical models [2] and [3]. The two-ray model shows multiple nulls of total field along the propagation path, causing the two-ray model to become invalid in certain propagation range (i.e., null field region). Both Weissberger model and Chen & Kua model show a large error of path loss prediction since the models are based on the wave propagation through a group of leaves. On the other hand, the proposed solution shows very good agreement for the range within a 50-meter limit, and such a solution is sufficiently good for designing a WSN in the orchard.

6. CONCLUSION

The path-loss prediction of radio wave propagation in an orchard using a modified UTD method has been proposed. The numerical procedure for path-loss prediction using the modified 3-D UTD solution for the impedance cylindrical surface together with the GB expansion via the CSP technique is presented in this paper. The UTD can efficiently deal with all kinds of scattered rays from the trees and the ground in the durian orchard. The UTD method provides the physical insight into the results. The study of the effects of field distribution using UTD (i.e., incident, reflected and scattered fields) on the total field is possible despite the fact that the effects cannot be computed by any other numerical method. The GB can be used to construct the source pattern that takes into account both the durian fruit and the antenna attached on the fruit. The numerical results manifest that the modified 3-D UTD for the impedance cylindrical surface can be used to accurately calculate the total field, under the assumption that the difference in height of transmitting and receiving antennas is within a few meters. The proposed numerical path-loss prediction procedure using the modified 3-D UTD solution will be efficiently used in various environments, such as in the network planning of the WSN in an orchard and in other settings for which the orchard physical dimensions are required.

ACKNOWLEDGMENT

The work of K. Phaebua was supported by the Thailand Research Fund (TRF) through the Royal Golden Jubilee Ph.D. Program under Grant No. PHD/0177/2550, while that of C. Phongcharoenpanich, M. Krairiksh and T. Lertwiriyaprapa was funded by the TRF through the Senior Research Scholar Program under Grant No. RTA5180002.

REFERENCES

1. Bertoni, H. L., *Radio Propagation for Modern Wireless Systems*, Prentice-Hall, New Jersey, 2000.
2. Azevedo, J. A. R. and F. E. S. Santos, "An empirical propagation model for forest environments at tree trunk level," *IEEE Trans. Antennas Propagat.*, Vol. 59, 2357–2367, 2011.
3. Meng, Y. S., Y. H. Lee, and B. C. Ng, "Study of propagation loss prediction in forest environment," *Progress In Electromagnetics Research*, Vol. 17, 117–133, 2009.
4. Gay-Fernandez, J. A., M. Garcia Sánchez, I. Cuinas, A. V. Alejos, J. G. Sanchez, and J. L. Miranda-Sierra, "Propagation analysis and deployment of a wireless sensor network in a forest," *Progress In Electromagnetics Research*, Vol. 106, 121–145, 2010.
5. Schettino, D. N., F. J. S. Moreira, and C. G. Rego, "Efficient ray tracing for radio channel characterization of urban scenarios," *IEEE Trans. Magn.*, Vol. 43, 1305–1308, 2007.
6. Pathak, P. H., "An asymptotic analysis of the scattering of plane waves by a smooth convex cylinder," *Radio Sci.*, Vol. 14, 419–435, 1979.
7. Pathak, P. H., W. D. Burnside, and R. J. Marhefka, "A uniform UTD analysis of the diffraction of electromagnetic waves by a smooth convex surface," *IEEE Trans. Antennas Propagat.*, Vol. 28, 609–622, 1980.
8. Pathak, P. H., "High-frequency techniques for antenna analysis," *Proc. IEEE*, Vol. 80, 44–65, 1992.
9. El-Sallabi, H. M. and P. Vainikainen, "Radio wave propagation in perpendicular streets of urban street grid for microcellular communications. Part I: channel modeling," *Progress In Electromagnetics Research*, Vol. 40, 229–254, 2003.
10. McNamara, D. A., C. W. I. Pistorius, and J. A. G. Malherbe, *Introduction to the Uniform Geometrical Theory of Diffraction*, Artech House, New York, 1990.
11. Li, Y. and H. Ling, "Numerical modeling and mechanism analysis

of VHF wave propagation in forested environments using the equivalent slab model," *Progress In Electromagnetics Research*, Vol. 91, 17–34, 2009.

12. Li, Y. and H. Ling, "Investigation of wave propagation in a dielectric rod array: Toward the understanding of HF/VHF propagation in a forest," *IEEE Trans. Antennas Propagat.*, Vol. 58, 4025–4032, 2010.
13. Koutitas, G. and C. Tzaras, "A UTD solution for multiple rounded surfaces," *IEEE Trans. Antennas Propagat.*, Vol. 54, 1277–1283, 2006.
14. Ghaddar, M., L. Talbi, T. A. Denidni, and A. Sebak, "A conducting cylinder for modeling human body presence in indoor propagation channel," *IEEE Trans. Antennas Propagat.*, Vol. 55, 3099–3103, 2007.
15. Phaebua, K., T. Lertwiriyaprapa, C. Phongcharoenpanich, and M. Krairiksh, "Path loss prediction in durian orchard using uniform geometrical theory of diffraction," *Proceedings of IEEE AP-S Int. Symp.*, 4 pages, 2009.
16. Lertwiriyaprapa, T., P. H. Pathak, and J. L. Volakis, "A UTD for predicting fields of sources near or on thin planar positive/negative material discontinuities," *Radio Sci.*, Vol. 42, RS6S18, 14 pages, 2007.
17. Lertwiriyaprapa, T., P. H. Pathak, and J. L. Volakis, "An approximate UTD ray solution for the radiation and scattering by antennas near a junction between two different thin planar material slab on ground plane," *Progress In Electromagnetics Research*, Vol. 102, 227–248, 2010.
18. Syed, H. H. and J. L. Volakis, "An asymptotic analysis of the plane wave scattering by a smooth convex impedance cylinder," Report, Radiation Laboratory Department of Electrical Engineering and Computer Science, The University of Michigan Ann Arbor, 1990.
19. Syed, H. H. and J. L. Volakis, "High-frequency scattering by a smooth coated cylinder simulated with generalized impedance boundary conditions," *Radio Sci.*, Vol. 26, 1305–1314, 1991.
20. Phaebua, K., T. Lertwiriyaprapa, C. Phongcharoenpanich, and P. H. Pathak, "A modified UTD solution for an impedance cylinder surface," *Proceedings of the Electrical Engineering/Electronics, Computer, Telecommunications, and Information Technology International Conference (ECTI-CON)*, 208–211, 2011.
21. Sim, Z. W., R. Shuttleworth, M. J. Alexander, and B. D. Grieve, "Compact patch antenna design for outdoor RF energy harvesting

in wireless sensor networks," *Progress In Electromagnetics Research*, Vol. 105, 273–294, 2010.

22. Pearson, L. W., "A scheme for automatic computation of fock-type integrals," *IEEE Trans. Antennas Propagat.*, Vol. 35, 1111–1118, 1987.
23. Rautio, J. C., "Reflection coefficient analysis of the effect of ground on antenna patterns," *IEEE Trans. Antennas Propagat.*, Vol. 29, 5–11, 1980.
24. Lertwiriyaprapa, T., K. Phaebua, C. Phongcharoenpanich, and M. Krairiksh, "Application of UTD ray solution for characterization of propagation in Thai commercial orchard," *Proceedings of Int. Conf. on Electromagn. in Adv. Appl.*, 176–179, 2010.
25. Lertwiriyaprapa, T., P. H. Pathak, K. Tap, and R. J. Burkholder, "Application of the complex source point method for analyzing the diffraction of an electromagnetic Gaussian beam by a curved wedge using UTD concepts," *Proceedings of IEEE AP-S Int. Symp.*, 4 pages, 2004.
26. Felsen, L. B., "Complex source point solution of the field equations and their relation to the propagation and scattering of Gaussian beams," *Symposia Mathematica*, Vol. 18, 39–56, 1975.
27. Tap, K., "Complex source point beam expansions for some electromagnetic radiation and scattering problems," Ph.D. dissertation, The Ohio State University, Columbus, OH, 2007.
28. Tokgoz, C., "Asymptotic high frequency analysis of the surface fields of a source excited circular cylinder with an impedance boundary condition," Ph.D. dissertation, The Ohio State University, Columbus, OH, 2002.
29. Sahin, H. and N. Ay, "Dielectric properties of hardwood species at microwave frequencies," *Journal of Wood Sci.*, Vol. 50, 375–380, 2004.
30. Peyskens, E., M. de Pourcq, M. Stevens, and J. Schalck, "Dielectric properties of softwood species at microwave frequencies," *Wood Sci. and Tech.*, Vol. 18, 267–280, 1984.
31. Ford, L. H. and R. Oliver, "An experimental investigation of the reflection and absorption of radiation of 9-cm. wavelength," *Proc. Phys. Soc.*, Vol. 58, 256–280, 1945.
32. Kim, H. S. and R. M. Narayanan, "A new measurement technique for obtaining the complex relative permittivity of terrain surfaces," *IEEE Trans. Geosci. Remote Sensing*, Vol. 40, 1190–1194, 2002.